ACADEMIC PRESS

Available online at www.sciencedirect.com
SCIENCE DIRECT®

Journal of Catalysis 217 (2003) 396–405

JOURNAL OF CATALYSIS

www.elsevier.com/locate/jcat

Kinetic studies of carbonylation of methanol to dimethyl carbonate over Cu^+X zeolite catalyst

Steven A. Anderson and Thatcher W. Root *

Department of Chemical Engineering, University of Wisconsin-Madison, Madison, WI 53706, USA

Received 8 November 2002; accepted 13 November 2002

Abstract

Direct synthesis of dimethyl carbonate offers prospects for a "green chemistry" replacement of phosgene use for polymer production and other processes. The carbonylation of methanol to produce dimethyl carbonate over a Cu^+X zeolite prepared by solid-state ion exchange has been investigated in a flow system at temperatures between 100 and 140 °C and a total pressure of 1 atm. Formation rates of dimethyl carbonate, methylal, and methyl formate are well described by a Langmuirian reaction mechanism, with quasi-equilibrated adsorption of methanol and oxidation of surface methanol to form methoxide, rate-limiting carbon monoxide insertion into the methoxide to form a carbomethoxide, and reaction of carbomethoxide with methoxide to form dimethyl carbonate. The by-products (methylal and methyl formate) are products of partial oxidation of the methoxide to formaldehyde. In situ FTIR experiments show the surface species present on the catalyst under reaction conditions and the effect of water on the system.

Keywords: Dimethyl carbonate; Methanol; Copper; Zeolite X; Carbonylation; Carbon monoxide; Chlorine elimination

1. Introduction

Dimethyl carbonate (DMC) has been drawing attention from researchers due to its use in replacing environmentally unfriendly compounds. DMC can be used as a methoxycarbonylation agent in place of phosgene for the production of polycarbonates and polyurethanes [1]. The use of DMC as a methylating agent in place of dimethyl sulfate and methyl halides has been well studied [1]. DMC has potential for use as a fuel additive due to its high oxygen content, good blending octane, and low toxicity [2]. DMC can also be blended with ethylene carbonate for use as an electrolyte in lithium-ion batteries [3].

Conventionally, DMC has been produced by reacting phosgene with methanol [1]. Because phosgene is highly toxic, a nonphosgene route to DMC is more desirable. The oxidative carbonylation of methanol

$$2CH_3OH + CO + \tfrac{1}{2}O_2 \rightarrow (CH_3O)_2CO + H_2O$$

has been pursued over a variety of carbon-supported cuprous chloride catalysts. In a liquid-phase slurry process using cuprous chloride as a catalyst conducted at approximately 120 °C and 27 atm, catalyst deactivation at high conversion levels limits the per-pass conversion to 20% [4,5].

A vapor-phase process for producing DMC would be more desirable, because the cuprous chloride is corrosive and deactivates in the liquid phase at high conversions [2]. Curnutt developed a vapor-phase process using a cupric chloride catalyst supported on activated carbon [6], but this catalyst deactivated by loss of chloride and required reactivation by drying and contact with gaseous HCl. Investigators have since examined this catalyst system to learn more about the catalyst structure and reaction kinetics [7–9].

King et al. [10] discovered that the chloride is not necessary to catalyze the reaction, and a solid catalyst prepared by supporting cuprous ions on a zeolite using the solid-state ion exchange method demonstrated good productivity and selectivity for DMC synthesis with little catalyst deactivation. Comparison of the Cu^+ zeolite catalysts with the cupric chloride catalysts has been done by King [11]. Under similar conditions, the Cu^+ zeolite catalysts were found to have higher activity per cm^3 of catalyst and higher selectivity for DMC formation. King also used in situ FTIR to elucidate the reaction mechanism by studying the surface species present under reaction conditions [11].

* Corresponding author.
E-mail address: thatcher@engr.wisc.edu (T.W. Root).

0021-9517/03/$ – see front matter
doi:10.1016/S0021-9517(02)00159-8

This paper presents the results of a steady-state kinetic study and an in situ FTIR study of the vapor-phase carbonylation of methanol over a copper zeolite catalyst. Screening experiments conducted with different zeolite supports, Si/Al ratios, copper exchange levels, and copper exchange techniques were conducted to identify a Cu^+X zeolite catalyst for the mechanistic study here. (The performance obtained from catalysts prepared by other procedures may be the subject of subsequent communications.) The results of the kinetic study demonstrate DMC production shows nearly first-order kinetics in carbon monoxide pressure, zero order in methanol pressure, slightly positive order in oxygen pressure, and -0.4 order in water pressure. The in situ FTIR study provides insight on how water decreases the reactivity of the catalyst.

2. Experimental section

2.1. Chemical reagents

The starting zeolite material was an ammonium X zeolite with a Si/Al ratio of 1.4 (Aldrich). Reagents included cuprous chloride (98+%, Aldrich), methanol (A.C.S. grade, Fisher Scientific), oxygen (Medical Grade, Praxair), nitrogen (99.998%, Praxair), air (21% O_2/79% N_2, Praxair), carbon monoxide (C.P. grade, Matheson), formaldehyde 37 wt% solution in H_2O (A.C.S. grade, Aldrich), and formic acid 88 wt% in H_2O (A.C.S. grade, Fisher).

2.2. Catalyst preparation

The Cu^+X zeolite was prepared by the solid-state ion exchange method, first described by Rabo et al. and Clearfield et al. [12–14]. Xie et al. applied this technique to prepare Cu(I)/zeolites for adsorption of carbon monoxide [15]. King et al. found that Cu(I)/zeolites prepared by this method are excellent catalysts for the vapor-phase carbonylation of methanol to form DMC [10]. The solid-state ion exchange procedure involves mixing the zeolite powder (ammonium or acid form) and the exchange cation compound (usually a metal halide) and heating to a high temperature in vacuum or an inert atmosphere. The process results in the formation of the metal zeolite and the evolution of gases. For example, the preparation of Cu^+X zeolite can be accomplished by mixing the ammonium X zeolite with CuCl powder. The mixture is heated, NH_3 and HCl gases evolve, and the Cu^+X zeolite powder is collected.

For the solid-state ion exchange method of preparation, a physical mixture of 0.9 g CuCl and 1.1 g ammonium X zeolite having a Si/Al ratio of 1.4 was packed into a stainless-steel tube having an inner diameter of 5 mm. This powder was heated in an argon stream at 625 °C for 16 h. The resulting Cu(I) zeolite was collected and used in experimental studies. The catalyst was light tan, indicating that the copper remained predominantly in the Cu(I) state. Inductively coupled plasma (ICP) elemental analysis of the treated catalyst determined that the final copper content was 30 wt%, corresponding to a Cu/Al ratio of 0.96. Turnover frequencies were calculated based on the copper content of the catalyst.

2.3. Apparatus and operation

Kinetic studies of methanol carbonylation were conducted using a stainless-steel tubular reactor with inner diameter 5 mm positioned in a temperature-controlled fluidized sand bath. In a typical run, 0.1–0.25 g of catalyst powder was packed into the reactor. Flowrates of nitrogen, oxygen, and carbon monoxide were set using mass flow controllers (MKS Instruments, Inc.). Methanol, water, formaldehyde, and formic acid flow rates were controlled by passing air through temperature-controlled bubblers. The total gas flow rate to the reactor was typically 20 cm^3/min. The experiments were carried out at atmospheric pressure.

The products leaving the reactor passed through a cold trap kept at -80 °C to collect liquid products for analysis using a Mattson Galaxy 5020 FT-IR spectrometer, typically using 256 scans with a resolution of 2 cm^{-1}. The IR cell used was a sealed liquid cell with CaF_2 windows and a pathlength of 0.05 mm (International Crystal Laboratories). After acquisition, spectra were deconvoluted into their components to quantify the reaction products.

2.4. In situ FTIR cell

All in situ FTIR spectra were obtained using an in situ FTIR cell as described by Yates and co-workers [16,17]. The cell was constructed within a standard stainless-steel tee having conflat flanges and commercial CaF_2 windows. The top port was sealed with a thermocouple/power feedthrough (Ceramaseal). Two stainless-steel tubes welded to the tee allowed gas flow through the cell.

The catalyst powder was pressed onto a photoetched tungsten grid (Buckabee Mears) using a hydraulic press at a pressure on the order of 10,000 psi. Excess catalyst was scraped from the grid after the pressing. The tungsten grid was then supported on copper clamps mounted on the copper rods of the thermocouple/power feedthrough. The temperature of the grid was controlled by resistive heating of the grid. The temperature was monitored with a Chromel–Alumel thermocouple spot-welded to the top center of the grid. Flows of nitrogen, oxygen, and carbon monoxide were set using mass flow controllers (MKS Instruments, Inc.). Methanol and water flow rates were controlled by flowing nitrogen or air through temperature-controlled bubblers. The in situ FTIR experiments were carried out at atmospheric pressure.

The spectra were taken using a Mattson Galaxy 5020 FT-IR spectrometer, typically using 128 scans with a reso-

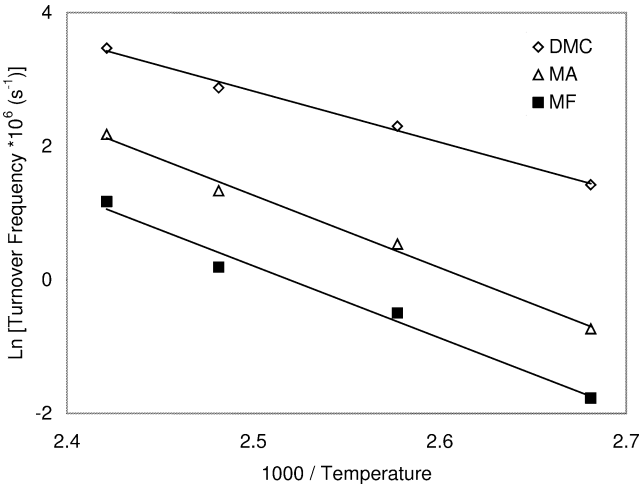

Fig. 1. Arrhenius plot of oxidative carbonylation of methanol over $Cu^{+}X$ zeolite. Reaction conditions: reaction temperature 100–140 °C; total pressure 1 atm; $CO/CH_3OH/N_2/O_2 = 5/2.5/4/1$.

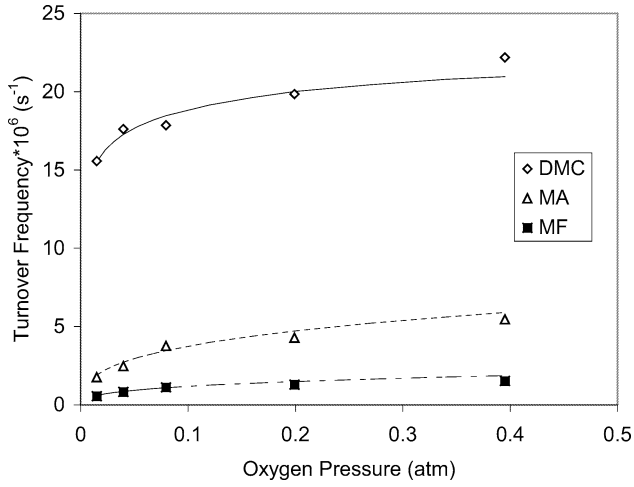

Fig. 3. Effect of oxygen pressure on oxidative carbonylation of methanol. Reaction conditions: reaction temperature 130 °C; carbon monoxide pressure 0.4 atm; methanol pressure 0.2 atm.

lution of 4 cm^{-1}. A background spectrum of the dry catalyst was taken prior to in situ experiments. After the reactant was introduced into the cell and a spectrum recorded, the dry catalyst spectrum was subtracted. IR spectra shown here display only the net spectral change of the surface of the catalyst.

3. Results

3.1. Reaction kinetics

Fig. 1 shows the effect of temperature on the rates of production of dimethyl carbonate (DMC), methyl formate (MF), and methylal (MA) over $Cu^{+}X$ zeolite. The apparent activation energies for DMC, MF, and MA production at these conditions were 64, 90, and 90 kJ/mol.

Figs. 2–6 show the dependence of the rates of production of DMC, MF, and MA on the pressure of carbon monoxide, oxygen, methanol, and water at 130 °C. The lines shown in Figs. 2–6 show the rates of reaction predicted using the methanol carbonylation mechanism described below under *Mechanism*.

Table 1 lists the apparent power-law reaction orders for the rates of formation of DMC, MF, and MA with respect to carbon monoxide, oxygen, methanol, and water determined from the data in Figs. 2–6. These power-law reaction orders are convenient for characterizing reactor performance in this parameter regime and also serve to guide development of the mechanism that follows.

Fig. 7 shows the effect of inlet formaldehyde pressure on the production of MF and MA. These data were collected with a methanol pressure of 0.17 atm, a water pressure of 0.004 atm, and an oxygen pressure of 0.08 atm. Adding formaldehyde to the feed had no effect on DMC production.

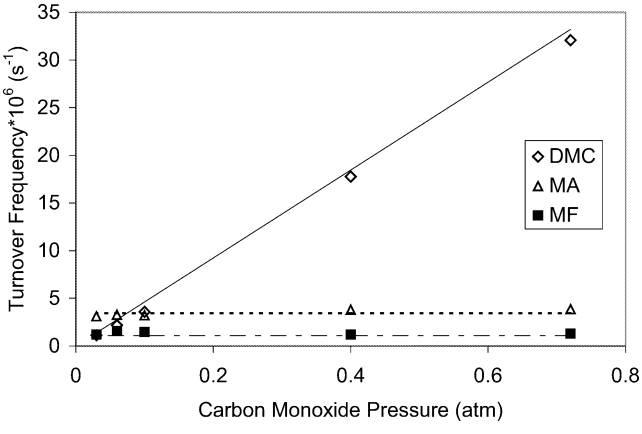

Fig. 2. Effect of carbon monoxide pressure on oxidative carbonylation of methanol. Reaction conditions: reaction temperature 130 °C; methanol pressure 0.2 atm; oxygen pressure 0.08 atm.

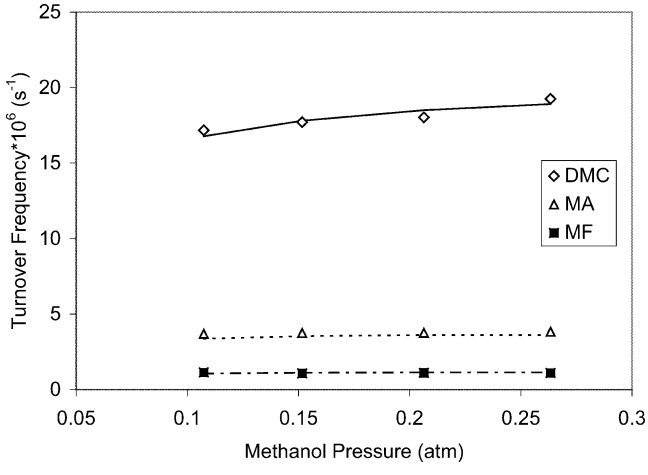

Fig. 4. Effect of methanol pressure on oxidative carbonylation of methanol. Reaction conditions: reaction temperature 130 °C; carbon monoxide pressure 0.4 atm; oxygen pressure 0.08 atm.

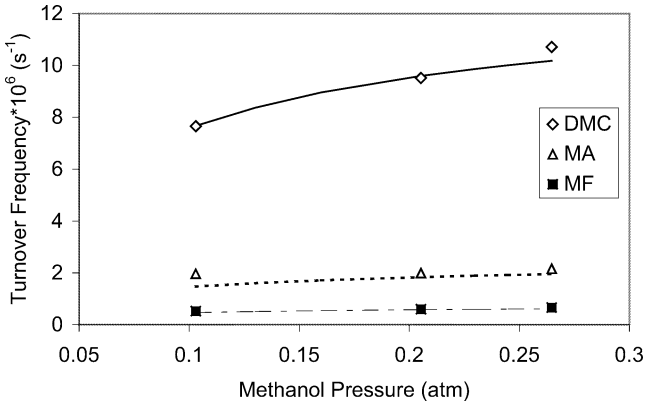

Fig. 5. Effect of methanol pressure on oxidative carbonylation of methanol with water fed to reactor. Reaction conditions: reaction temperature 130 °C; carbon monoxide pressure 0.4 atm; oxygen pressure 0.08 atm; water pressure 0.005 atm.

3.2. In situ FTIR adsorption isotherm results

3.2.1. Water adsorption

Equilibrium water adsorption on a fresh Cu^+X zeolite sample has been studied at two different water pressures, 0.0023 and 0.0074 atm, and a wide range of temperatures. For example, Fig. 8 shows the adsorbed water bending mode peak (1640 cm^{-1}) and how its intensity varies with sample temperature under a constant water vapor pressure of 0.0074 atm. Under equilibrium conditions at a constant H_2O pressure, the Langmuir adsorption equilibrium expression can be rearranged to obtain the form

$$K_{eq} = \theta_{H_2O}/P_{H_2O}(1-\theta_{H_2O}). \quad (1)$$

The coverage of water on the surface of the catalyst has been calculated using the approximation that the area under the IR peak is proportional to the amount of water adsorbed on the catalyst surface, using the equation

$$\theta_{H_2O} = A_{H_2O}/A^{max}_{H_2O}, \quad (2)$$

where A_{H_2O} is the area under the 1640 cm^{-1} peak and $A^{max}_{H_2O}$ is the area corresponding to 100% coverage, determined by fitting the data taken at two pressures to Eq. (1) to minimize the difference in the equilibrium constant calculated for the data with multiple water pressures at the same temperature. The highest observed peak area corresponded to 90% coverage relative to the fitted $A^{max}_{H_2O}$.

Using the Van't Hoff equation, the enthalpy for water adsorption on Cu^+X zeolite can be estimated from the variation of $\ln K_{eq}$ with $1/T$:

$$\Delta H_{ads} = R\frac{d(\ln K_{eq})}{d(1/T)}. \quad (3)$$

Fig. 9 shows the Van't Hoff plot for the adsorption of water at two different pressures, illustrating the consistency of results from this approach. The heat of adsorption for water on the catalyst determined by this method is 57.4 ± 1.1 kJ/mol, and the equilibrium constant can be fitted to $K_{eq}(T) = 3.1 \times 10^{-6}\exp(6900/T)$ atm^{-1}.

Equilibrium water adsorption on ammonium X zeolite was studied at a water pressure of 0.0069 atm. Fig. 10 shows the Van't Hoff plot for the adsorption of water on ammonium X zeolite. The heat of adsorption for water on ammonium X zeolite determined by this method is 45.3 ± 1.7 kJ/mol. This lower heat of adsorption of water on ammonium X zeolite compared to Cu^+X zeolite indicates Cu^+ ions play an active role in water adsorption on Cu^+X zeolite.

Table 1
Reaction orders for DMC, MA, and MF production

Reactant	Reaction Orders		
	DMC	MA	MF
Carbon monoxide	1.1	0.1	0
Oxygen	0.1	0.3	0.3
Methanol (without water in feed)	0.1	0	0
Methanol ($P_{H_2O} = 0.005$ atm)	0.3	0.1	0.2
Water	−0.4	−0.3	−0.3

3.2.2. Methanol adsorption

Methanol adsorption on a fresh Cu^+X zeolite sample has been studied at two pressures, 0.048 and 0.0082 atm. A series of IR spectra showing the methanol δ_{CH} mode at

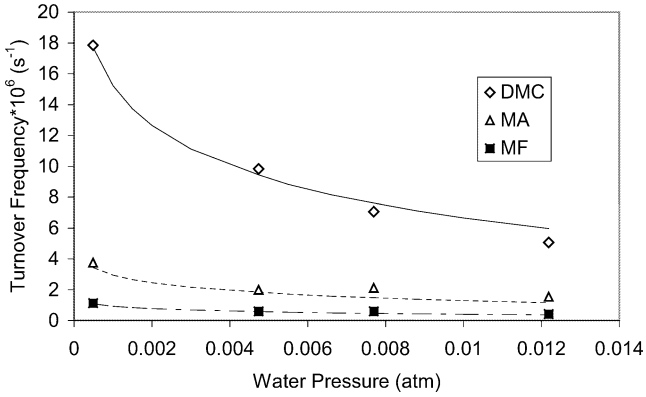

Fig. 6. Effect of water pressure on oxidative carbonylation of methanol. Reaction conditions: reaction temperature 130 °C; carbon monoxide pressure 0.38 atm; oxygen pressure 0.08 atm; methanol pressure 0.22 atm.

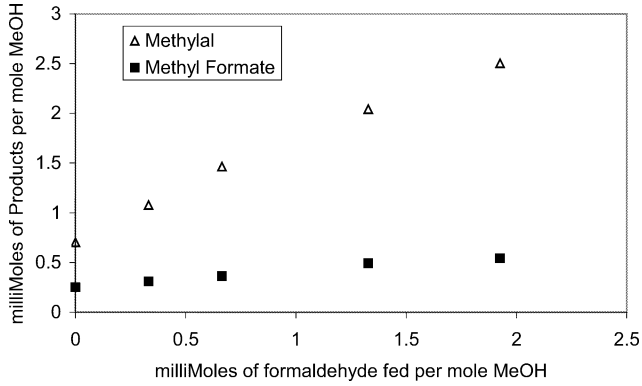

Fig. 7. Effect of formaldehyde on production of methylal and methyl formate. Reaction conditions: reaction temperature 130 °C; methanol pressure 0.2 atm; oxygen pressure 0.08 atm; water pressure 0.005 atm.

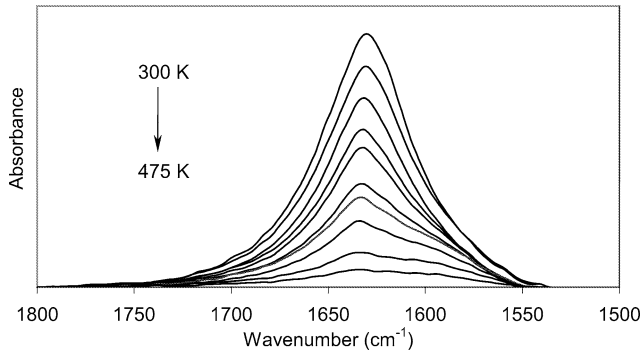

Fig. 8. Infrared spectra of water adsorbed onto Cu^+X zeolite, showing the 1640 cm^{-1} bending mode. Water pressure maintained at 0.0074 atm.

1458 cm^{-1} was recorded as a function of sample temperature at a methanol pressure of 0.048 atm, shown in Fig. 11. Unfortunately, the adsorption in the C–H stretching region (2700–3000 cm^{-1}) of the gas phase methanol present in the cell obscures the adsorption from the surface species, so no information on surface species is obtained in this range. The heat of adsorption for methanol calculated from the Van't Hoff plot shown in Fig. 12 is 39.5 ± 1.9 kJ/mol, and the equilibrium constant for nondissociative methanol adsorption can be fitted to $K_{eq}(T) = 8.6 \times 10^{-5} \exp(4760/T)$ atm^{-1}.

3.2.3. Methanol and methoxide coverage

Methanol adsorption on Cu^+X zeolite catalyst at 130 °C has been studied in the presence of both oxygen and water to allow oxidative dehydrogenation and formation of surface methoxide. The catalyst was exposed to an atmosphere containing methanol, oxygen, and water, and the gas composition and temperature were kept constant for 30 min to allow the surface to equilibrate. After equilibration, the cell was purged with nitrogen at a flow rate of 2000 cm^3/min and a series of FTIR spectra were taken with the catalyst surface maintained at 130 °C.

For the spectra shown in Figs. 13 and 14, the surface was equilibrated for 30 min with a grid temperature of 130 °C and 0.2 atm methanol, 0.08 atm oxygen, and 0.005 atm

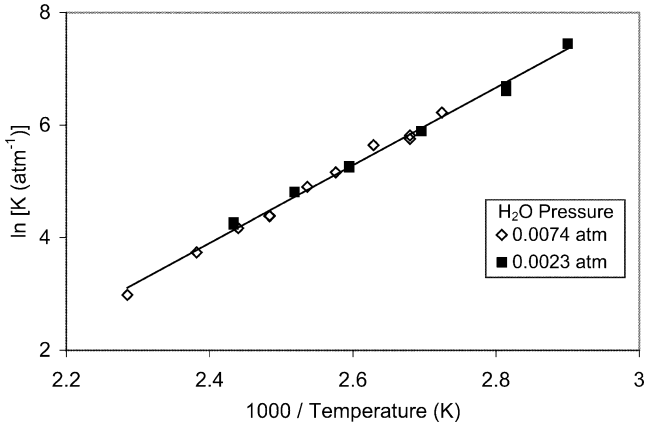

Fig. 9. Van't Hoff plot of water adsorption onto Cu^+X zeolite.

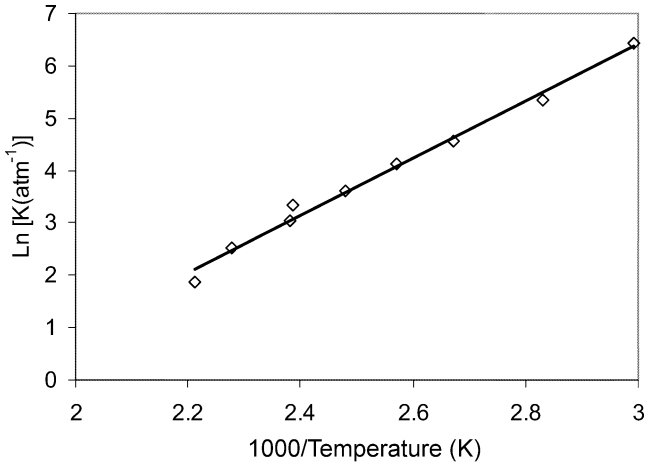

Fig. 10. Van't Hoff plot of water adsorption onto ammonium X zeolite.

water. Fig. 13 shows IR spectra of the methanol/methoxide region (1340–1540 cm^{-1}) as a function of time, and Fig. 14 shows the initial and final spectra of the C–H stretching region (2700–3000 cm^{-1}). King assigned the peaks of the C–H stretching region for methanol and methoxide adsorbed on Cu(I)Y zeolite [11]. Methanol shows an asymmetric C–H stretch and a symmetric C–H stretch at 2955 and 2847 cm^{-1}. Surface methoxide shows these two stretching frequencies red-shifted to 2932 and 2826 cm^{-1}. The spectra in Fig. 14 show that the intensity of the bands that correspond to surface methanol decrease with time, while the bands that correspond to surface methoxide do not decrease with time during the nitrogen purge.

Fig. 13 shows that during the nitrogen purge the spectral area decreases with time; the rate at which the area decreases with time slows and a significant portion of the area remains after more than 20 min. This shows that a significant portion of methanol adsorbed on the catalyst surface desorbs relatively quickly, while a fraction of adsorbed species do

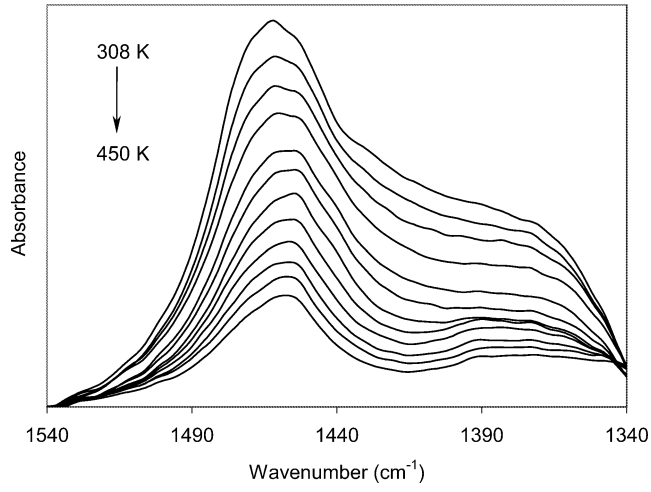

Fig. 11. Infrared spectra of methanol adsorbed onto Cu^+X zeolite, showing the δ_{CH} mode at 1458 cm^{-1}.

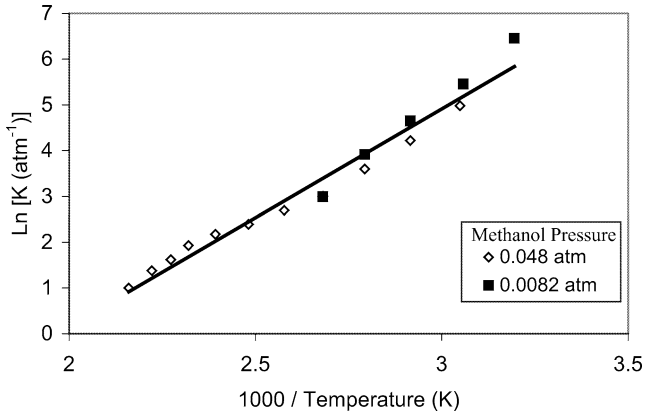

Fig. 12. Van't Hoff plot of methanol adsorption onto Cu^+X zeolite.

not desorb; the latter are assigned to be surface methoxide that is irreversibly adsorbed under these conditions.

Fig. 15 shows the decrease in area under the methanol/methoxide (1458 cm^{-1}) curve as the time increases for several different initial conditions. Increasing the water pressure decreases the amount of surface methoxide as well as the initial amount of methanol and methoxide on the surface. Increasing the oxygen pressure does not affect the initial total amount of methanol and methoxide on the surface of the catalyst, but does increase the amount of methoxide left on the surface during the desorption period.

4. Mechanism

The liquid-phase carbonylation of methanol over Cu(I) from cuprous chloride has been shown by Romano et al. [4] to occur in the following steps:

$$2CH_3OH + \tfrac{1}{2}O_2 + 2Cu^+Cl^- \rightarrow 2(CH_3O\text{–}Cu)^+Cl^- + H_2O,$$

$$2(CH_3O\text{–}Cu)^+Cl^- + CO \rightarrow (CH_3O)CO + 2Cu^+Cl^-.$$

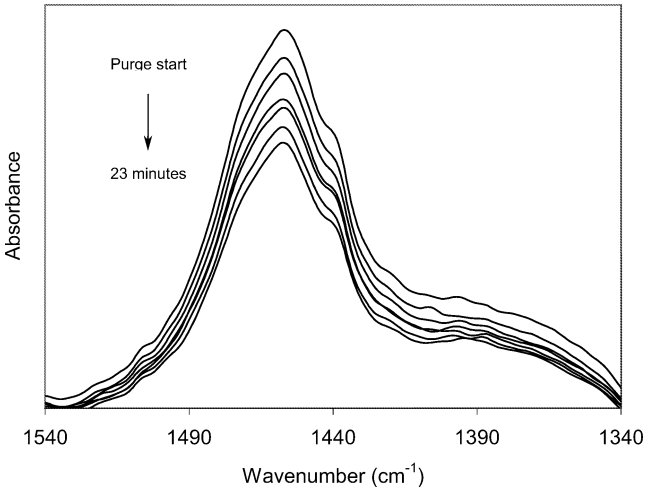

Fig. 13. Infrared spectra of methanol and methoxide on Cu^+X zeolite, showing the δ_{CH} mode at 1458 cm^{-1} at 130 °C during nitrogen purge.

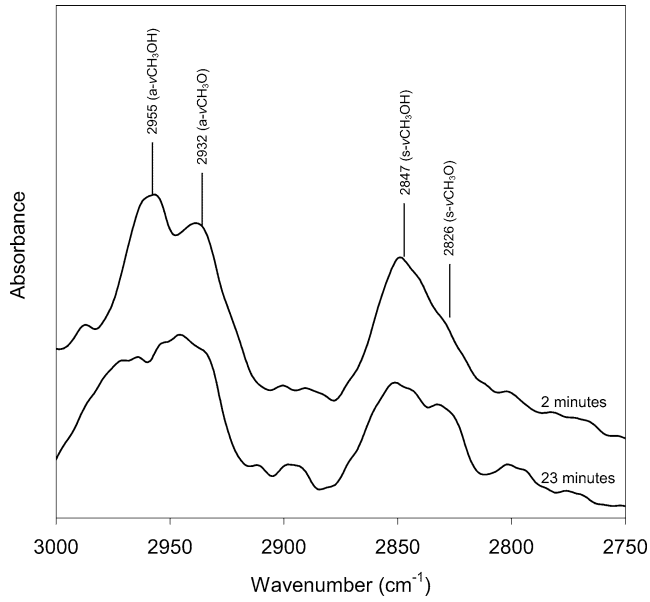

Fig. 14. C–H stretching region of methanol/methoxide on the surface of Cu^+X zeolite during cell purge at 130 °C.

King has shown that the oxidative carbonylation of methanol to DMC carried out using a Cu(I) zeolite can be separated into a similar three step mechanism, with the zeolite framework charge (Ze^-) acting in the same manner as the chloride ion [11]:

$$2CH_3OH + \tfrac{1}{2}O_2 + 2Cu^+Ze^- \rightarrow 2(CH_3O\text{–}Cu)^+Ze^- + H_2O,$$

$$(CH_3O\text{–}Cu)^+Ze^- + CO \rightarrow (CH_3O\text{–}CO\text{–}Cu)^+Ze^-,$$

$$2(CH_3OCO\text{–}Cu) + Ze^- + 2CH_3OH + \tfrac{1}{2}O_2 \rightarrow 2(CH_3O)_2CO + H_2O + 2Cu^+Ze^-.$$

The in situ FTIR data in Fig. 13 show that adsorbed methanol and surface methoxide both account for significant coverage on the catalyst surface when methanol and oxygen

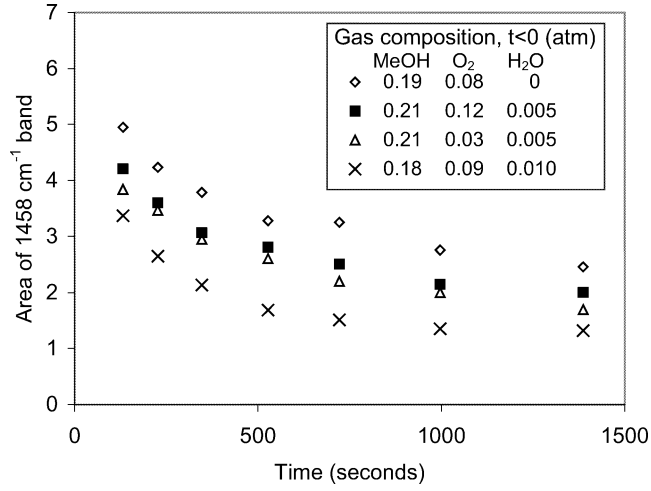

Fig. 15. Area of 1458 cm^{-1} δ_{CH} band during nitrogen purge at 130 °C.

are present in the environment of the catalyst at 130 °C. The first step of the mechanism proposed by King can be split into two equilibrated steps to account for both species present on the catalyst surface. Here, the * represents the active site (Cu^+Ze^-). Step (R5) and beyond will be described in the following elaboration:

$$CH_3OH + {}^* \leftrightarrow CH_3OH^*, \quad \text{(R1)}$$

$$CH_3OH^* + \tfrac{1}{4}O_2 \leftrightarrow CH_3O^* + \tfrac{1}{2}H_2O, \quad \text{(R2)}$$

$$CH_3O^* + CO \leftrightarrow CH_3OCO^*, \quad \text{(R3)}$$

$$CH_3OCO^* + CH_3O^* \leftrightarrow (CH_3O)_2CO + 2^*, \quad \text{(R4)}$$

$$2CH_3O^* + \tfrac{1}{2}O_2 \leftrightarrow 2CH_2O^* + H_2O, \quad \text{(R5)}$$

$$CH_2O^* \leftrightarrow CH_2O + {}^*, \quad \text{(R6)}$$

$$CH_2O + 2CH_3OH \leftrightarrow (CH_3O)_2CH_2 + H_2O, \quad \text{(R7)}$$

$$CH_2O + \tfrac{1}{2}O_2 \leftrightarrow HCOOH, \quad \text{(R8)}$$

$$CHOOH + CH_3OH \leftrightarrow CHOOCH_3 + H_2O, \quad \text{(R9)}$$

$$H_2O + {}^* \leftrightarrow H_2O^*. \quad \text{(R10)}$$

Steps (R1)–(R4) provide the basic mechanism for DMC formation. The first step of the mechanism is the adsorption of methanol onto a copper site of the zeolite. The second reaction of this mechanism is not an elementary step, but is the sum of several rapid elementary steps that result in the equilibrium formation of methoxide. In previous work, the present steps (R1) and (R2) have been combined into a single lumped step. King showed that methanol adsorbs and reacts quickly with oxygen to form methoxide [11], demonstrating that the initial steps of this mechanism are equilibrated under reaction conditions. The third step is insertion of carbon monoxide to form carbomethoxide, and this step is rate-limiting for DMC production. Romano et al. suggested carbon monoxide insertion as the rate-limiting step in their liquid phase system as well [4]. King has shown FTIR spectra that can be interpreted as formation of carbomethoxide [11]. In the fourth step the carbomethoxide reacts with additional methoxide to form DMC. King has shown that the carbomethoxide reacts quickly to form DMC when methanol and oxygen are also in the system [11], which leads to the conclusion that step (R4) occurs rapidly when steps (R1) and (R2) are equilibrated and adequate methoxide is present.

Steps (R5)–(R9) provide for formation of the two major by-products. The key intermediate in the generation of methylal and methyl formate is the formaldehyde produced by the oxidation of surface methoxide. This is not unexpected, because the oxidation of methanol to formaldehyde over copper catalysts has been known for more than a century [18]. If the oxidation of surface methoxide is the rate-limiting step for formaldehyde formation and the formaldehyde formed reacts quickly with the abundant methanol to form the by-products, it will not be detected in the reactor effluent. Evidence that formaldehyde is such a reactive intermediate is seen in Fig. 7, which shows that adding formaldehyde to the feed to the Cu^+X zeolite generates additional methylal and methyl formate, with 1 mole of product generated per mole formaldehyde fed to the reactor and no formaldehyde detected in the reactor effluent.

Masamoto and Matsuzaki demonstrated that formaldehyde can react with methanol (step (R7)) over an acid catalyst to produce methylal [19]. This individual reaction has been verified in our lab by passing methanol, formaldehyde, and air over a copper-free H–X zeolite at 130 °C. It was observed that 1 mole of methylal was formed for every mole of formaldehyde fed, and no methyl formate was observed. All of the formaldehyde fed to the reactor was consumed. The methylal formation that occurs using Cu^+X zeolite as a catalyst is likely to be the result of formaldehyde reacting with methanol over the residual H^+ sites of the zeolite that are present due to incomplete copper exchange during solid-state ion exchange.

Formic acid production, from formaldehyde oxidation, has been postulated as a precursor to methyl formate production over $CuCl_2$ supported on carbon catalysts [7,11] and CuCl/MCM-41 [20]. This indicates that the production of formic acid from formaldehyde may occur over defect copper sites in the Cu^+X zeolite, those defect sites possibly being Cu^0 sites produced during catalyst preparation. The role of formic acid as an intermediate to methyl formate production has been verified by flowing formic acid, methanol, and air through the reactor at 130 °C without catalyst, under conditions similar to the reaction conditions. One mole of formic acid was consumed per mole methyl formate produced, and all the formic acid fed to the reactor was consumed.

Water significantly decreases the reaction rates over the Cu^+X zeolite catalyst, as shown in Fig. 6. One cause for this rate reduction is the effect of water on the equilibrium of step (R2), which decreases the methoxide coverage on copper sites. Additionally, in situ FTIR spectroscopy experiments show that water can adsorb onto the Cu^+X zeolite catalyst, preventing the formation of methoxide on the reactive sites. This site-blocking effect of water has been included via step (R10). Water is produced in steps (R2), (R7), and (R9) of the reaction mechanism, so water will always be present in increasing amounts as the reaction proceeds.

A methanol carbonylation mechanism should explain the observed kinetic orders of DMC, MF, and MA production. King [11] established that the slow step along the route for DMC production is the carbon monoxide insertion (step (R3)). The results of adding formaldehyde into the feed show evidence that formaldehyde gas reacts very quickly, which leads to the conclusion that the formation of formaldehyde in step (R5) is the rate-limiting step toward the production of MA and MF. Therefore, we treat steps (R1), (R2), and (R10) as quasi-equilibrated and model steps (R4) and (R6)–(R9) as being at steady state. The

formaldehyde formed in step (R5) reacts to form either MA or MF in step (R7) or step (R8). Lacking detailed information on the kinetics of these minor steps, the relative amounts of each product will be described by coefficients ϕ_{MA} and ϕ_{MF}, with $\phi_{MA} = r_7/(r_7 + r_8)$ and $\phi_{MF} = r_8/(r_7 + r_8)$, where r_7 and r_8 are the rates of steps (R7) and (R8), respectively. This series of assumptions for the methanol carbonylation mechanism leads to the following rate expressions for the methanol carbonylation reactions,

$$R_{DMC} = k_3 P_{CO} \theta_{CH_3O}, \tag{4}$$

$$R_{MA} = \phi_{MA} R_{Form} = \phi_{MA} k_5 P_{O_2}^{1/4} \theta_{CH_3O}, \tag{5}$$

$$R_{MF} = \phi_{MF} R_{Form} = \phi_{MF} k_5 P_{O_2}^{1/4} \theta_{CH_3O}, \tag{6}$$

where R_{DMC}, R_{MF}, R_{MA}, and R_{Form} represent the rates of formation of DMC, MF, MA, and formaldehyde, k_3 is the rate constant for the forward reaction of step (3), ϕ_{MA} and ϕ_{MF} describe the selectivities of MA and MF production from formaldehyde, and θ_{CH_3O} is the fraction of methoxide sites on the catalyst surface. The reverse reactions for the slow steps may be neglected both because of the low conversion and the thermodynamic equilibrium of the overall reactions highly favoring the formation of products under the reaction conditions.

The three most abundant surface intermediates are adsorbed methanol, surface methoxide, and adsorbed water. The coverages of carbomethoxide and adsorbed DMC are insignificant under these conditions [11]. The surface coverage of the methoxide species is dependent on the equilibrium of step (R2), the surface coverage of methanol on the catalyst, and the gas phase pressures of oxygen and water. Therefore, θ_* can be determined from the equation

$$\theta_* = 1 - (\theta_{CH_3OH} + \theta_{CH_3O} + \theta_{H_2O}) = \left[1 + K_1 P_{MeOH} + \frac{K_1 K_2 P_{MeOH} P_{O_2}^{1/4}}{P_{H_2O}^{1/2}} + K_{10} P_{H_2O}\right]^{-1}. \tag{7}$$

The combination of the equations which describe the surface species with Eqs. (4), (5), and (6) provide expressions for the rates of formation of DMC, MA, and MF:

$$R_{DMC} = \frac{k_3 K_1 K_2 P_{MeOH} P_{CO} P_{O_2}^{1/4} / P_{H_2O}^{1/2}}{\left[1 + K_1 P_{MeOH} + \frac{K_1 K_2 P_{MeOH} P_{O_2}^{1/4}}{P_{H_2O}^{1/2}} + K_{10} P_{H_2O}\right]}, \tag{8}$$

$$R_{MA} = \frac{\phi_{MA} k_5 K_1 K_2 P_{MeOH} P_{O_2}^{1/2} / P_{H_2O}^{1/2}}{\left[1 + K_1 P_{MeOH} + \frac{K_1 K_2 P_{MeOH} P_{O_2}^{1/4}}{P_{H_2O}^{1/2}} + K_{10} P_{H_2O}\right]}, \tag{9}$$

$$R_{MF} = \frac{\phi_{MF} k_5 K_1 K_2 P_{MeOH} P_{O_2}^{1/2} / P_{H_2O}^{1/2}}{\left[1 + K_1 P_{MeOH} + \frac{K_1 K_2 P_{MeOH} P_{O_2}^{1/4}}{P_{H_2O}^{1/2}} + K_{10} P_{H_2O}\right]}. \tag{10}$$

Table 2
Fitted parameters for oxidative carbonylation mechanism at 130 °C

Parameter	Value and units	Fit with
k_3	$(7.35 \pm 0.61) \times 10^{-5}$ atm^{-1} s^{-1}	Kinetic data
K_1	11.57 atm^{-1}	In situ FTIR
K_2	0.102 ± 0.021 atm$^{0.25}$	Kinetic data
K_{10}	84.6 atm^{-1}	In situ FTIR
k_5	$(1.36 \pm 0.04) \times 10^{-5}$ atm$^{-0.25}$ s^{-1}	Kinetic data
ϕ_{MA}	0.760 ± 0.016	Kinetic data

The values for this set of parameters were determined using the Athena Visual Workbench [21]. This software employs a general regression analysis of the kinetic data with the reactor modeled as a continuous stirred-tank reactor. The analysis used an average reactor water pressure based on the feed water pressure and half the contribution of water generated by the measured overall reaction rates of all products, which varied slightly with methanol conversion and reaction selectivity. The values for methanol and water adsorption constants (K_1 and K_{10}) have been determined using in situ FTIR spectroscopy, and were not adjusted during the general regression analysis, leaving four parameters (k_3, k_5, ϕ_{MA}, and K_2) that were fitted to the data using linear regression analysis. (ϕ_{MF} is not an independent parameter, since $\phi_{MF} = 1 - \phi_{MA}$.)

The lines shown in Figs. 2–6 show the rates of reaction predicted using the rate expressions for DMC, MA, and MF and the fitted parameters listed in Table 2. The predicted rates provide a good fit to the experimental data, with an average relative error of 7.3% for DMC production, 12.5% for methylal, and 11.7% for methyl formate.

5. Discussion

The reactivity and selectivity of the Cu^+X zeolite catalyst indicate that it is a promising catalyst for DMC production by the oxidative carbonylation of methanol. The rate of DMC production over Cu^+X compares well with the rate of production over a Cu^+Y having 7.1 wt% Cu [11]. Under similar reaction conditions, the Cu^+Y catalyst has a turnover frequency of 8.0×10^{-5} s^{-1} [11], while the Cu^+X has a turnover frequency of 2.0×10^{-5} s^{-1}. Accounting for the higher copper content of the Cu^+X catalyst, which is more than four times larger than the Cu^+Y reported by King, shows that these catalysts perform with similar activity based on catalyst mass. The selectivity of both catalysts is similar as well.

Increasing the temperature increases the rate of DMC production and decreases the selectivity to DMC based on methanol. This study did not determine the full temperature dependence of all fitted rate parameters.

The nearly first-order kinetics in carbon monoxide pressure observed for the production of dimethyl carbonate indicate that the rate-limiting step for this reaction is the CO insertion into the methoxide species. This result also indi-

cates that the carbon monoxide is not present at significant surface coverage, and is consistent with carbon monoxide reacting with surface methoxide via either an Eley–Rideal or Langmuir–Hinshelwood surface step. This mechanism also provides that the carbon monoxide pressure has no effect on the production of methylal and methyl formate. Results from a microcalorimetric study of carbon monoxide adsorption on Cu–Y zeolite [22] indicate that carbon monoxide is not strongly bonded to the copper ions at the reaction conditions of this study, consistent with these interpretations.

The near-zero reaction order with respect to methanol pressure for the DMC reaction rate indicates that the surface is nearly covered with methanol and methoxide. The nonnegative reaction order for methanol and the nearly first-order kinetics for DMC formation with respect to carbon monoxide pressure indicate that carbon monoxide is not competing for sites under these conditions and that the carbon monoxide insertion into the methoxide species (step (R3)) occurs via an Eley–Rideal reaction. The positive order in oxygen pressure for DMC production indicates that oxygen affects the equilibrium of step (R2) in the reaction and that increasing the oxygen pressure increases the ratio of surface methoxide to adsorbed methanol. The by-product formation rate shows an oxygen dependence that is $\frac{1}{4}$ order higher than the DMC rate dependence on oxygen pressure, as a result of the oxidation of the methoxide species to the adsorbed formaldehyde species being the rate-limiting step to by-product formation. The formaldehyde species reacts quickly to form methyl formate or methylal and is not an abundant surface species or an observed byproduct.

The rate of production of DMC is -0.4 order with respect to water pressure. As shown in Fig. 6, the mechanism predicts the decrease in reactivity of the catalyst with increasing water pressure well. The form of the model equation (Eq. (8)) allows the water dependence on the reaction rate to vary from 0 to -1.5 order, depending on surface species coverage.

Fig. 16 shows the dependence of the methanol, water, and methoxide coverage of the surface of the catalyst with respect to water pressure predicted by the model using the values of the parameters in Table 2. The effect of water on the equilibrium of step (R2) is responsible for the decrease in rate as the water pressure increases from 0.0005 to 0.015 atm, seen by the fivefold decrease (from 2.5 to 0.5) of the methoxide to methanol ratio. Water adsorption on the catalyst surface is insignificant compared to the effect water has on the equilibrium of surface methoxide formation (step (R2)) at low partial pressures (0 to 0.01 atm). As the water partial pressure increases above 0.01 atm, the coverages of methanol and methoxide decrease as water begins to occupy a significant fraction of the catalyst surface. Clearly, water inhibition can be important, and this will be the subject of future study.

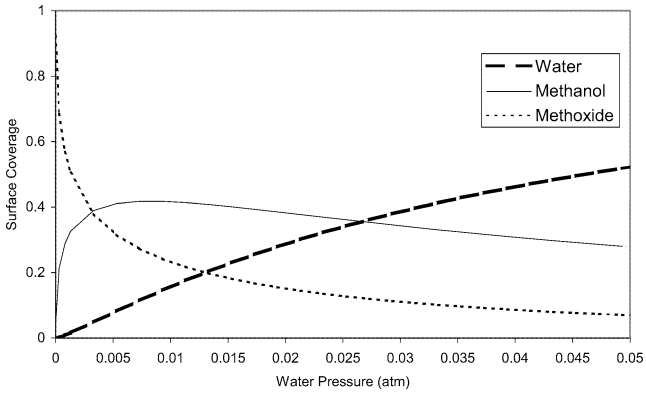

Fig. 16. Surface coverage of $Cu^{+}X$ zeolite predicted by kinetic mechanism using the values from Table 2. Oxygen pressure 0.08 atm; methanol pressure 0.22 atm.

The effect of the methanol pressure on the reactivity of the catalyst when water is in the system at a constant pressure of 0.005 atm has been measured to verify that the water at this pressure is affecting the equilibrium of surface methoxide formation and not blocking sites by adsorption. Fig. 5 shows that the rates of product formation have a slight positive dependence on methanol pressure, which the mechanism predicts well. Water adsorption on the catalyst sites would have caused a much higher methanol dependence on the reaction rates, counter to what is seen experimentally.

The model predicts the DMC production rate and selectivity will increase as the carbon monoxide pressure of the system increases. Preliminary studies have shown that the selectivity to DMC based on methanol is above 90% at carbon monoxide pressures on the order of 4 atm. The effect of carbon monoxide pressure on the system at elevated pressures is now under examination.

6. Conclusions

The steady-state kinetic data agrees well with a reaction mechanism that posits slow insertion of carbon monoxide into the methoxide species. This kinetic model contains six independent parameters. The fitted values of these parameters indicate that the most abundant surface species on the catalyst is methoxide at low water pressures.

Water inhibits the production of dimethyl carbonate by decreasing the surface coverage of methoxide on the catalyst surface. The important effect water has on this system at low water pressure is shifting the equilibrium of methoxide formation from methanol and oxygen. As the water pressure increases, the equilibrium shifts from surface methoxide towards adsorbed methanol. At higher pressures water adsorbs onto catalyst sites, directly blocking them and decreasing the availability of sites for the adsorption of methanol and subsequent reactions.

Acknowledgment

We gratefully acknowledge the financial support of the National Science Foundation Training Grant for the program

“Catalysis for Environmentally Conscious Manufacturing” (HER-9554586).

References

[1] Y. Ono, Appl. Catal. A Gen. 155 (1997) 133.
[2] M.A. Pacheco, C.L. Marshall, Energy Fuel 11 (1997) 2.
[3] S. Megahed, W. Ebner, J. Power Sources 54 (1) (1995) 155.
[4] U. Romano, R. Tesel, M.M. Mauri, P. Rebora, Ind. Eng. Chem. Prod. Res. Dev. 19 (1980) 396.
[5] U. Romano, Chim. Ind. (Milan) 75 (4) (1993) 303.
[6] G.L. Curnutt, US Patent 5004827, 1991.
[7] K. Tomishige, T. Sakaihori, S. Sakai, K. Fujimoto, Appl. Catal. A Gen. 181 (1999) 95.
[8] M. Zinbin, Z. Renzhe, X. Genhui, H. Fei, C. Hongfang, Catal. Today 30 (1996) 201.
[9] Y.J. Wang, Y.Q. Zhao, B.G. Yuan, B.C. Zhang, J.S. Cong, Appl. Catal. A Gen. 171 (2) (1998) 255.
[10] S.T. King, M.E. Jones, M.M. Olken, US Patent 5391803, 1995.
[11] S.T. King, J. Catal. 161 (1996) 530.
[12] J.A. Rabo, M.L. Poutsma, G.W. Skeels, in: J.W. Hightower (Ed.), Proceedings, 5th International Congress on Catalysis, Palm Beach (1972), North-Holland, Amsterdam, 1973, p. 1353.
[13] J.A. Rabo, in: Zeolite Chemistry and Catalysis, in: ACS Monograph, Vol. 171, Am. Chem. Society, Washington, DC, 1976, p. 332.
[14] A. Clearfield, C.H. Saldarriaga, R.C. Buckley, in: J.B. Uytterhoeven (Ed.), Proceedings, 3rd International Congress on Molecular Sieves, Zurich (1973), University of Leuven Press, 1973, p. 241.
[15] Y.C. Xie, N.Y. Bu, J. Liu, G. Yang, J.G. Qiu, N.F. Yang, Y. Tang, US Patent 4917711, 1990.
[16] T.H. Ballinger, J.C.S. Wong, J.T. Yates Jr., Langmuir 8 (1992) 1676.
[17] T.P. Beebe, P. Gelin, J.T. Yates Jr., Surf. Sci. 148 (2–3) (1984) 526.
[18] J.K. Dixon, J.E. Longfield, in: P.H. Emmet (Ed.), Catalysis, Vol. 7, Reinhold, New York, 1960, pp. 231–236.
[19] J. Masamoto, K. Matsuzaki, J. Chem. Eng. Jpn. 27 (1) (1994) 1.
[20] Z. Li, K. Xie, R.C.T. Slade, Appl. Catal. A Gen. 205 (2001) 85.
[21] M.C. Caracotsios, W.E. Stewart, Athena Visual Workbench 8.2, Stewart and Associates, Madison, WI, 2002.
[22] G.D. Borgard, S. Molvik, P. Balaraman, T.W. Root, J.A. Dumesic, Langmuir 11 (6) (1995) 2065.